

A Two-Dimensional Energy Surface for a Type II S_N2 Reaction in Aqueous Solution[†]

Jiali Gao* and Xinfu Xia

Contribution from the Department of Chemistry, State University of New York at Buffalo, Buffalo, New York 14214

Received May 19, 1993*

Abstract: The role of aqueous solvation on the potential surface of the S_N2 Menshutkin reaction between ammonia and methyl chloride has been examined by using a combined quantum mechanical and statistical mechanical method. In the present simulation approach, the reactant molecules are treated by the semiempirical AM1 theory, while the solvent is represented by the empirical TIP3P model. Solute-solvent interactions are evaluated through Hartree-Fock molecular orbital calculations throughout the fluid simulation. In this paper, it is first demonstrated, by comparison with high-level ab initio results, that this hybrid quantum mechanical and molecular mechanical (QM/MM-AM1/TIP3P) model can provide an adequate description of intermolecular interactions between the solute and solvent for the Menshutkin reaction. The free energy surface in aqueous solution is then determined via statistical perturbation theory with a grid search algorithm. The results suggest that the solvent effects strongly stabilize the transition state and products. The computed free energy of activation (26 kcal/mol) is in good agreement with previous theoretical and experimental estimates. The most striking finding is that the transition state is shifted significantly toward the reactants, with a lengthening of the C-N bond by 0.30 Å and a shortening of the C-Cl bond by 0.15 Å. This is in accord with the Hammond postulate and consistent with previous theoretical studies. Analyses of the simulation results indicate that the charge separation during the present Type II S_N2 reaction is promoted by the solvent effect, with a charge transfer of about 65% complete at the transition state. Detailed insights into the structural and energetic nature of the differential solvation of the reactants and transition state are provided.

Introduction

The bimolecular nucleophilic substitution reaction is one of the most fundamental processes in organic chemistry and has attracted numerous experimental and theoretical investigations.¹⁻³ In his classic work, Ingold classified nucleophilic substitutions into four categories according to the charge type of the nucleophile, being negative or neutral, and of the substrate, being neutral or positive.¹ This classification has helped qualitatively to explain the dramatic solvent effect on the rate of S_N2 reactions observed experimentally on the basis of charge distributions of the reactant and the transition state.¹⁻⁴ Quantitative characterization of the solute-solvent interaction at the molecular level, however, was only recently made possible, thanks to advances in computer technology and accurate free energy computational techniques. In particular, much attention has been paid to the prototypical Type I S_N2 reaction of Cl⁻ + CH₃Cl → ClCH₃ + Cl⁻, involving an anion and a neutral substrate in aqueous and organic solvents.⁵⁻⁹ To further our understanding of the solvation effect on S_N2 reactions, extension of theory to other charge types is warranted.

Much progress has been made in elucidating the intrinsic properties of gas-phase S_N2 reactions through quantum mechanical ab initio calculations. The double-well potential energy surface for the Type I reaction⁹ predicted by early theoretical studies was confirmed by the extensive experimental work of Brauman and co-workers.^{10,11} In addition, ab initio calculations provide valuable information on the transition-state (TS) structure and charge distributions along the whole reaction coordinate. Recently, these computations have been extended to condensed-phase simulations using statistical mechanical Monte Carlo and molecular dynamics techniques.⁵⁻⁸ This was led by the calculation of the reaction profile involving chloride and methyl chloride in aqueous and DMF solutions.^{5a} The striking solvent effect observed

[†] Taken in part from the Ph.D. dissertation of X.X., SUNY, Buffalo, 1993.

* Abstract published in *Advance ACS Abstracts*, October 1, 1993.

(1) (a) Ingold, C. K. *Structure and Mechanism in Organic Chemistry*, 2nd ed.; Cornell University Press: Ithaca, NY, 1969. (b) Hughes, E. D.; Ingold, C. K. *J. Chem. Soc.* **1935**, 244.

(2) (a) Harris, J. M.; McManus, S. P., Eds.; *Nucleophilicity*; American Chemical Society: Washington, DC, 1987; Series 215. (b) Hartshorn, S. R. *Aliphatic Nucleophilic Substitution*; Cambridge University Press: London, 1973. (c) Hines, J. *Physical Organic Chemistry*; McGraw-Hill: New York, 1962. (d) Ritchie, C. D. In *Solute-Solvent Interactions*; Goetzee, J. F., Ritchie, C. D., Eds.; Marcel Dekker: New York, 1969; p 284.

(3) Dewar, M. J. S.; Dougherty, R. C. *The PMO Theory of Organic Chemistry*; Plenum Press: New York, 1975.

(4) (a) Menshutkin, N. Z. *Phys. Chem.* **1890**, 5, 589. (b) Parker, A. J. *Chem. Rev.* **1969**, 69, 1. (c) Abraham, M. H.; Greillier, P. L.; Abboud, J. M.; Doherty, R. M.; Taft, R. W. *Can. J. Chem.* **1988**, 66, 2673. (d) Abboud, J. M.; Notario, R.; Bertran, J.; Solà, M. *Prog. Phys. Org. Chem.* **1993**, 19, 1.

(5) (a) Chandrasekhar, J.; Smith, S. F.; Jorgensen, W. L. *J. Am. Chem. Soc.* **1984**, 106, 3049; **1985**, 107, 154. (b) Chandrasekhar, J.; Jorgensen, W. L. *J. Am. Chem. Soc.* **1985**, 107, 2974. (c) Jorgensen, W. L.; Buckner, J. K. *J. Phys. Chem.* **1986**, 90, 4651.

(6) (a) Chiles, R. A.; Rossky, P. J. *J. Am. Chem. Soc.* **1984**, 106, 6867. (b) Huston, S. E.; Rossky, P. J.; Zichi, D. A. *J. Am. Chem. Soc.* **1989**, 111, 5680. (c) Bash, P. A.; Field, M. J.; Karplus, M. *J. Am. Chem. Soc.* **1987**, 109, 8092. (d) Hwang, J.; King, G.; Creighton, S.; Warshel, A. J. *J. Am. Chem. Soc.* **1988**, 110, 5297.

(7) (a) Bergsma, J. P.; Gertner, B. J.; Wilson, K. R.; Hynes, J. T. *J. Chem. Phys.* **1987**, 86, 1356. (b) Gertner, B. J.; Whitnell, R. M.; Wilson, K. R.; Hynes, J. T. *J. Am. Chem. Soc.* **1991**, 113, 74. (c) Gertner, B. J.; Wilson, K. R.; Hynes, J. T. *J. Chem. Phys.* **1989**, 90, 3537. (d) Kozaki, T.; Morihashi, K.; Kikuchi, O. *J. Am. Chem. Soc.* **1989**, 111, 1547. (e) Basilevsky, M. V.; Chudinov, G. E.; Napolov, D. V. *J. Phys. Chem.* **1993**, 97, 3270.

(8) (a) Tucker, S. C.; Truhlar, D. G. *J. Phys. Chem.* **1989**, 93, 8138. (b) Tucker, S. C.; Truhlar, D. G. *J. Am. Chem. Soc.* **1990**, 112, 3347.

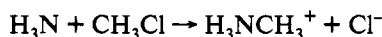
(9) (a) Wolfe, S.; Mitchell, D. J.; Schlegel, H. B. *J. Am. Chem. Soc.* **1981**, 103, 7602, 7694. (b) Dedieu, A.; Veillar, G. A. *J. Am. Chem. Soc.* **1972**, 94, 6730. (c) Bader, R. F. W.; Duke, A. J.; Messer, P. R. *J. Am. Chem. Soc.* **1973**, 95, 7715. (d) Carrion, F.; Dewar, M. J. S. *J. Am. Chem. Soc.* **1984**, 106, 3531. (e) Vande Linde, S. G.; Hase, W. L. *J. Phys. Chem.* **1990**, 94, 2778. (f) Shi, Z.; Boyd, R. J. *J. Am. Chem. Soc.* **1990**, 112, 6789. (g) Shaik, S. S.; Schlegel, H. B.; Wolfe, S. *Theoretical Aspects of Physical Organic Chemistry. The S_N2 Mechanism*; Wiley: New York, 1992.

(10) (a) Olmstead, W. N.; Brauman, J. I. *J. Am. Chem. Soc.* **1977**, 99, 4019. (b) Pellerite, M. J.; Brauman, J. I. *J. Am. Chem. Soc.* **1980**, 102, 5993. (c) Bohme, D. K.; Young, L. B. *J. Am. Chem. Soc.* **1974**, 96, 4027. (d) Gronert, S.; DePuy, C. H.; Bierbaum, V. M. *J. Am. Chem. Soc.* **1991**, 113, 4009.

(11) (a) Graul, S. T.; Bowers, M. T. *J. Am. Chem. Soc.* **1991**, 113, 9696. (b) Cyr, D. M.; Posey, L. A.; Bishea, G. A.; Han, C.-C.; Johnson, M. A. *J. Am. Chem. Soc.* **1991**, 113, 9697. (c) Wilbur, J. L.; Brauman, J. I. *J. Am. Chem. Soc.* **1991**, 113, 9699.

experimentally was demonstrated by a predicted increase of 15 kcal/mol in activation free energy over its intrinsic (*in vacuo*) barrier.⁵

In the present study, we report the results of a theoretical examination of a Type II S_N2 reaction, the Menshutkin reaction in aqueous solution,^{1,4a}



using the combined quantum mechanical and molecular mechanical (QM/MM) Monte Carlo simulation method described previously.¹² Several issues are of interest in this reaction. First, TS structures are generally expected to be different in the gas phase and in solution. This is not a serious problem for symmetric reactions because the solvent effects are the same on both sides of the TS along the reaction coordinate. Thus, the structural change is not expected to be considerably large and has been confirmed by Jorgensen and Buckner for the Type I reaction in water.^{5c} However, switching to a system consisting of a neutral nucleophile and substrate (Type II), in which large charge separation occurs during the reaction, should yield an "uneven" solvation effect that is accompanied by a reduction of the reaction barrier and a shift in the TS structure according to the Hammond postulate.¹³ In a recent communication, we reported the results of a study of the Menshutkin reaction using empirical potential functions.¹⁴ That work, along with the study of Solà et al.,¹⁵ confirmed the empirical expectation and demonstrated that the solvent effect can, indeed, significantly modify the position of the transition state. Consequently, the solvent effect should be included in the electronic structure calculations to determine the reaction path in solution. Second, the solvent effect on the polarization of the reactants is expected to enhance the charge separation of the Menshutkin reaction over that of the reaction in the gas phase.^{14,15} Although this would be very difficult to investigate using empirical potential functions, the problem is naturally solved by the QM/MM method because the solvent effect is coupled into the electronic structure calculation in fluid simulations.^{13,16} Therefore, additional insights into the solvent effect may be inferred from the QM/MM simulation. Finally, it is desirable to locate the minimum free energy path for the Menshutkin reaction in solution rather than to follow the reaction path of the gas-phase process.^{5-9,14}

In this report, we have extended our study to cover the free energy surface of the Menshutkin reaction by mapping out the bond formation and breaking process independently. The results provide new insights into the structure and energetics for the understanding of S_N2 reactions in solution. In the following, computational details are given first, followed by results and discussion.

Computational Details

(a) Intermolecular Potential Functions. In the present study, we adopt a combined QM/MM approach in statistical mechanical Monte Carlo simulations. The method has been reviewed recently by several authors; additional details are in ref 12. Here, the fluid system is partitioned into a quantum mechanical region consisting of the solute molecule, H₃N-CH₃-Cl, and a molecular mechanical region containing solvent monomers which are approximated by the three-site TIP3P model for water.^{16,19}

(12) For reviews, see: (a) Field, M. J.; Bash, P. A.; Karplus, M. *J. Comput. Chem.* **1990**, *11*, 700. (b) Luzhkov, V.; Warshel, A. *J. Comput. Chem.* **1992**, *13*, 199. (c) Gao, J. *J. Phys. Chem.* **1992**, *96*, 537. Methods using continuum models such as the self-consistent reaction field theory are also relevant but are not specifically discussed. For recent applications and leading references, see: (d) Cramer, C. J.; Truhlar, D. G. *J. Am. Chem. Soc.* **1991**, *113*, 8305. (e) Karelson, M. M.; Zerner, M. C. *J. Phys. Chem.* **1992**, *96*, 6949.

(13) See, for example: (a) Issacs, N. S. *Physical Organic Chemistry*; John Wiley & Sons, Inc.: New York, 1987. (b) Connors, K. A. *Chemical Kinetics: The Study of Reaction Rates in Solution*; VCH: New York, 1990.

(14) Gao, J. *J. Am. Chem. Soc.* **1991**, *113*, 7796.

(15) Solà, M.; Lledos, A.; Duran, M.; Bertran, J.; Abboud, J. M. *J. Am. Chem. Soc.* **1991**, *113*, 2873.

(16) Gao, J.; Xia, X. *Science* **1992**, *258*, 631.

Table I. Lennard-Jones Parameters Used in the AM1/TIP3P Model

atom	σ , Å	ϵ , kcal/mol
	H ₃ N-CH ₃ -Cl	
C	3.4000	0.1000
N	3.0875	0.1615
Cl	4.1964	0.1119
H _C	2.0000	0.0700
H _N	0.0	0.0
	Water	
O	3.1506	0.1521
H	0.0	0.0

Clearly, to compute the energies of the QM solute molecule throughout the condensed-phase simulation, a computationally efficient method must be used. Therefore, the semiempirical Austin Model 1 (AM1) theory developed by Dewar and co-workers¹⁷ is employed to form the AM1/TIP3P force field in this study.^{12a,c} Warshel and co-workers have used the empirical valence bond (EVB) theory in their study of the Type I S_N2 reaction and enzymatic processes.^{6a,12b}

For the QM region, the solute is represented by valence electrons and nuclei. The restricted Hartree-Fock wave function, Φ , is used with a single Slater determinant of all doubly occupied molecular orbitals (MOs), which are linear combinations of a minimum basis set.^{17,18} The total effective Hamiltonian of the system is given by¹²

$$\hat{H}_{\text{eff}} = \hat{H}^{\circ} + \hat{H}_{\text{QM/MM}} + \hat{H}_{\text{MM}} \quad (1)$$

where \hat{H}° is the AM1 Hamiltonian for the solute molecule, \hat{H}_{MM} is the molecular mechanical solvent energy, and $\hat{H}_{\text{QM/MM}}$ is the solute-solvent interaction Hamiltonian (eq 2),

$$\begin{aligned} \hat{H}_{\text{QM/MM}} &= \hat{H}_{\text{QM/MM}}^{\text{el}} + \hat{H}_{\text{QM/MM}}^{\text{vdW}} \\ &= \left(-\sum_{s=1}^S \sum_{i=1}^{2N} \frac{eq_s}{r_{si}} + \sum_{s=1}^S \sum_{m=1}^M \frac{q_s Z_m}{R_{sm}} \right) + \\ &\quad \sum_{s=1}^S \sum_{m=1}^M 4\epsilon_{sm} \left[\left(\frac{\sigma_{sm}}{R_{sm}} \right)^{12} - \left(\frac{\sigma_{sm}}{R_{sm}} \right)^6 \right] \quad (2) \end{aligned}$$

where e is the charge of electrons, q_s and Z_m are charges on the solvent and solute nuclei, S and M are the corresponding total numbers of interaction sites, and r_{si} and R_{sm} are the distances of the solute electrons and nuclei from the solvent sites, respectively. The Lennard-Jones term in eq 2 accounts for the dispersion interaction between the QM and MM regions, which are omitted in the hybrid QM/MM approximation;¹⁶ it contains the only adjustable parameters for the solute (σ_m and ϵ_m) in the present approach. These parameters are listed in Table I. The combining rules used for the solute-solvent interaction are $\sigma_{sm} = (\sigma_s \sigma_m)^{1/2}$ and $\epsilon_{sm} = (\epsilon_s \epsilon_m)^{1/2}$.

The total potential energy in the combined QM/MM force field is computed using eq 3,

$$E_{\text{tot}} = \langle \Phi | \hat{H}_{\text{eff}} | \Phi \rangle = E_{\text{QM}} + E_{\text{QM/MM}}^{\text{el}} + E_{\text{QM/MM}}^{\text{vdW}} + E_{\text{MM}} \quad (3)$$

Here, Φ is the wave function of the solute in aqueous solution, E_{MM} is the MM pair interaction energy for the solvent molecules enumerated with the empirical TIP3P potential, and $(E_{\text{QM}} + E_{\text{QM/MM}}^{\text{el}})$ is determined through Hartree-Fock self-consistent-field (SCF) MO calculations.

As usual, the intermolecular interaction energy for a water dimer in the MM region is given as the sum of Coulombic interactions between all atomic pairs plus a Lennard-Jones term between the two oxygen atoms (eq 4). The three-site TIP3P model is employed for water, with experimental geometry held fixed throughout the simulations.¹⁹

$$\Delta E_{ab} = \sum_i \sum_j \sum_k \sum_l (q_i q_j / r_{ij}) + 4\epsilon_{00} [(\sigma_{00}/r_{00})^{12} - (\sigma_{00}/r_{00})^6] \quad (4)$$

(b) Geometrical Constraints. Due to the symmetry of the Menshutkin reaction of H₃N + CH₃Cl, the three non-hydrogen atoms, N, C, and Cl,

(17) Dewar, M. J. S.; Zoebisch, E. G.; Healy, E. F.; Stewart, J. J. P. *J. Am. Chem. Soc.* **1985**, *107*, 3902.

(18) Hehre, W. J.; Radom, L.; Schleyer, P. v. R.; Pople, J. A. *Ab Initio Molecular Orbital Theory*; Wiley: New York, 1986.

(19) Jorgensen, W. L.; Chandrasekhar, J.; Madura, J. D.; Impey, R. W.; Klein, M. L. *J. Chem. Phys.* **1983**, *79*, 926.

are constrained to be collinear along the C_3 symmetry axis. Dihedral variations of H_3N and CH_3 groups about the C–N bond are allowed during the Monte Carlo simulation.^{20b} The bond length and bond angles associated with the hydrogen atoms are optimized at a fixed H–N–C–H dihedral angle sampled in the calculation.

(c) **Monte Carlo Simulations.** Statistical mechanical Monte Carlo calculations were carried out in the isothermal–isobaric (NPT) ensemble at 25 °C and 1 atm.²⁰ A cubic box containing 265 water molecules (ca. $20 \times 20 \times 20 \text{ \AA}^3$) was used in the free energy surface calculation, whereas a rectangular box consisting of 321 water molecules (ca. $19 \times 19 \times 28 \text{ \AA}^3$) was employed for computing the reaction profile (see below) to allow adequate sampling at large separation distances along the reaction coordinate (RC). In the latter simulation, the C_3 symmetry axis is oriented to coincide with the z-axis of the water box. Standard Metropolis sampling procedures were adopted along with the Owicki–Scherraga preferential sampling technique using $1/(r^2 + c)$ weighting, where $c = 150 \text{ \AA}^2$, to facilitate the statistics near the solute molecule.²¹ At least 5×10^5 configurations were taken in the equilibration stage for each point on the free energy surface, while 10^6 configurations were collected to compute the statistical averages. The solute–solvent interaction energy was evaluated by single-point Hartree–Fock SCF calculations using the effective Hamiltonian of eq 1. The intermolecular interactions are feathered to zero between spherical cutoff distances of 9.0 and 9.5 Å for water–water and solute–water interactions, based roughly on the center-of-mass separation. New configurations were generated by randomly selecting a molecule, translating it in all three Cartesian directions, rotating it along a randomly chosen axis, and varying the internal rotation. An acceptance rate of about 40% was maintained by using ranges of $\pm 0.11 \text{ \AA}$ and 10° for molecular motions. Volume changes were restricted to within $\pm 100 \text{ \AA}^3$ at every 1625 configurations. Standard deviations are estimated from averages of blocks 10^5 configurations.

(d) **Free Energy Surface.** In order to assess the solvent effects on the TS structure of the prototypical Menshutkin reaction, $H_3N + CH_3Cl \rightarrow CH_3NH_3^+ + Cl^-$, in aqueous solution, a two-dimensional free energy surface was constructed through a grid search method. The two independent coordinates of the map are C–N distance R_{CN} and C–Cl distance R_{CCl} . The grid searching was carried out in a rectangular region of $1.406 \text{ \AA} \leq R_{CN} \leq 2.406 \text{ \AA}$ and $1.744 \text{ \AA} \leq R_{CCl} \leq 2.444 \text{ \AA}$, while statistical perturbation theory was used to compute free energy differences between neighboring grid points.²² Specifically, at a given value of R_{CCl} , a series of perturbation calculations with $\Delta R_{CN} = \pm 0.05 \text{ \AA}$ were carried out to yield a free energy profile as a function of R_{CN} . The relative heights of two such neighboring profiles (parallel to each other) at an interval of 0.10 \AA were determined by another perturbation calculation with respect to R_{CCl} at a fixed R_{CN} value. Finally, the potential surface was anchored relative to the free energy at an RC of -2.0 \AA (see below). Hence, the whole free energy surface was constructed (Figure 1) through a total of 87 simulations. The numerical results are summarized in the supplementary material.

We note that Warshel and co-workers introduced an elaborate method that employs a mapping function to drive the reactant state to the product state.^{64,12b,23} The free energy of activation for the reaction is then recovered by an umbrella-sampling-type treatment,²⁴ making use of the energy gap, $\Delta\epsilon$, between the products and reactants on the mapping function potential surface as the reaction coordinate.^{64,23b} The method is particularly advantageous for use with the EVB approach, which has been applied to many chemical and biological systems by these authors.²³ The method, of course, can be used with the MO approach as described in ref 12b. Effectively, the method gives the probability of reaching the

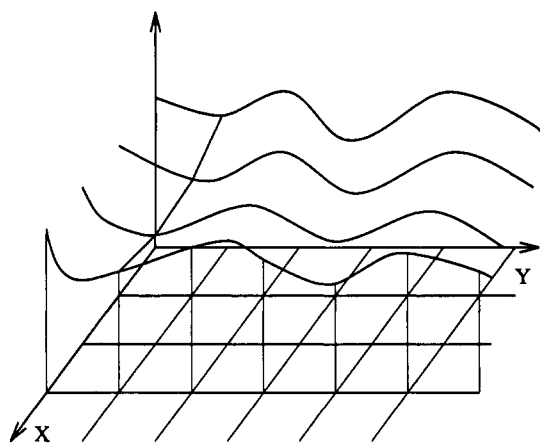


Figure 1. Schematic representation of the algorithm used in calculating the free energy map. X represents the C–Cl distance, and Y is the C–N separation in the Menshutkin reaction. In the first step, free energy profiles in the Y direction are constructed by perturbing Y with fixed X values. These profiles are then connected by perturbations with respect to X.

transition state from the reactant state, while the energy of the transition state (which is defined by $\Delta\epsilon$) results from a distribution of solute geometries in solution. Thus, structural constraints are not involved in these calculations, though the mapping function provides an energetic restriction. On the other hand, the present grid approach, as in many applications reported in the literature,^{5,6} yields the potential of mean force for the reaction if a one-dimensional reaction coordinate is used or the solvent-averaged free energy surface with a multiple-dimensional reaction coordinate.

Recently, Pearlman and Kollman proposed a method for establishing the free energy surface using statistical perturbation theory.²⁵ They suggested perturbing the two independent variables, the dihedral angles in their study, in multiple directions. Consequently, several free energy changes can be obtained from a single fluid simulation. This would, indeed, be computationally efficient if empirical potentials are used because the time-limiting step is the configurational sampling in those simulations. However, the major cost in the hybrid QM/MM method is the quantum mechanical MO calculations. Furthermore, multiple-direction mutations over the present double-wide sampling²⁶ will also significantly increase the memory requirement in the combined QM/MM method. Thus, the grid search in the present study is limited to double-wide sampling.²⁶

Gas-Phase Reaction

(a) **Potential Surface in the Gas Phase.** In our previous study,¹⁴ the transition-state structure for the Menshutkin reaction of $H_3N + CH_3Cl \rightarrow CH_3NH_3^+ + Cl^-$ was located through ab initio molecular orbital calculations at the 6-31 + G(d) level using GAUSSIAN 90.²⁷ A minimum energy path (MEP) was then determined by energy minimizations at different values of the reaction coordinate (RC) defined by¹⁴

$$RC = R_{CCl} - R_{CN} - RC_0 \quad (5)$$

where R_{CCl} and R_{CN} are respectively the distances of Cl and N from C, and RC_0 is the difference between the C–Cl and C–N separations at the saddle point. A C_{3v} symmetry was maintained during the minimizations. Correlation energies were obtained by single-point energy computations at the MP4SDTQ/6-31 + G(d) level for all structures considered. The gas-phase free energy profile was constructed using standard procedures by including zero-point energy and entropy corrections based on the 6-31 + G(d) vibrational frequencies.¹⁴ In these calculations, ab initio vibrational frequencies were scaled by a factor of 0.89, and the

(20) All simulations were performed using (a) MCQUB (Monte Carlo QM/MM at University at Buffalo, Gao, J., SUNY at Buffalo, 1992) and (b) BOSS (Version 2.9; Jorgensen, W. L., Yale University, 1990) programs. (c) The quantum mechanical energy was evaluated with MOPAC (Stewart, J. J. P. MOPAC, Version 5; Quantum Chemistry Program Exchange 455, 1986, Vol. 6, No. 391).

(21) (a) Owicki, J. C.; Scherraga, H. A. *Chem. Phys. Lett.* **1977**, *47*, 600. (b) Owicki, J. C. *ACS Symp. Ser.* **1978**, *86*, 159. (c) Jorgensen, W. L.; Bigot, B.; Chandrasekhar, J. *J. Am. Chem. Soc.* **1982**, *104*, 4584.

(22) Zwanzig, R. W. *J. Chem. Phys.* **1954**, *22*, 1420. (23) (a) Warshel, A. *J. Phys. Chem.* **1979**, *83*, 1640. (b) Hwang, J.-K.; Warshel, A. *J. Am. Chem. Soc.* **1987**, *109*, 715. (c) Warshel, A.; Sussman, F.; Hwang, J.-K. *J. Mol. Biol.* **1988**, *201*, 139. (d) Warshel, A.; Aqvist, J. *Annu. Rev. Biophys. Chem.* **1991**, *20*, 267. (e) Warshel, A. *Curr. Opin. Struct. Biol.* **1992**, *2*, 230. (f) Warshel, A. *Computer Modeling of Chemical Reactions in Enzymes and Solutions*; Wiley: New York, 1991.

(24) (a) Patey, G. N.; Valleau, J. P. *J. Chem. Phys.* **1975**, *63*, 2334. (b) Valleau, J. P.; Torrie, G. M. In *Statistical Mechanics, Part A: Equilibrium Techniques*; Berne, B. J., Ed.; Plenum: New York, 1977; p 169.

(25) Pearlman, D. A.; Kollman, P. A. *J. Am. Chem. Soc.* **1991**, *113*, 7167.

(26) Jorgensen, W. L.; Ravimohan, C. *J. Chem. Phys.* **1985**, *83*, 3050.

(27) Frisch, M. J.; Head-Gordon, M.; Trucks, G. W.; Foreman, J. B.; Schlegel, H. B.; Raghavachari, K.; Robb, M.; Binkley, J. S.; Gonzalez, C.; Defrees, D. J.; Fox, D. J.; Whiteside, R. A.; Seeger, R.; Melius, C. F.; Baker, J.; Martin, R. L.; Kahn, L. R.; Stewart, J. J. P.; Topiol, S.; Pople, J. A. *GAUSSIAN 90*; Gaussian Inc.: Pittsburgh, PA, 1990.

Table II. Computed and Experimental Energies for the Menshutkin Reaction in the Gas Phase at 25 °C (kcal/mol)

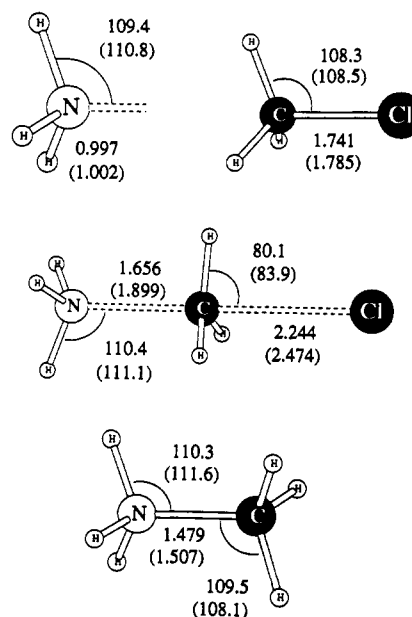
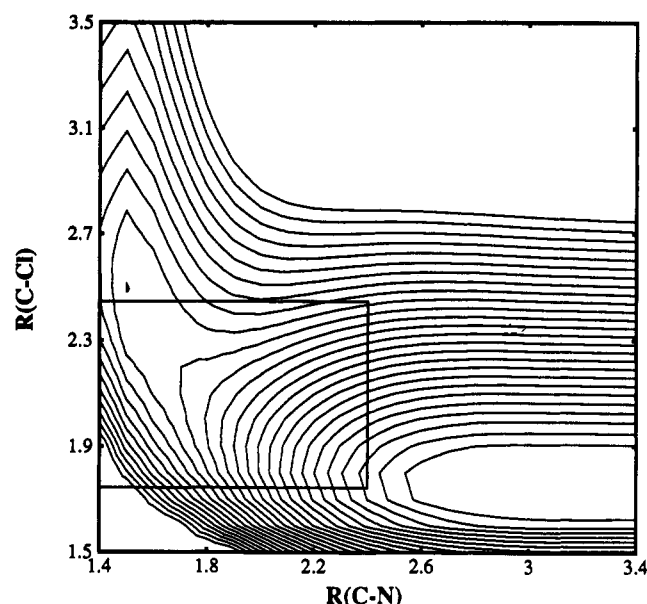
species	ΔH (AM1)	ΔG (MP4/6-31+G*) ^a	ΔG (expt) ^a
H ₃ N + CH ₃ Cl	0	0	0
[H ₃ N-CH ₃ -Cl] [‡]	50.0	46.7	
CH ₃ NH ₃ ⁺ + Cl ⁻	137	119	110

^a Reference 14.

resulting vibrations that are lower than 500 cm⁻¹ were treated as rotations. In addition, the normal mode along the reaction coordinate, which becomes imaginary at the TS, was ignored. The computed free energy of reaction is in good agreement with the experimental data (Table II).^{14,28} It should be pointed out that the reaction path calculated this way is not necessarily the steepest descent path (SDP) due to the restriction of eq 5. The SDP or the intrinsic reaction coordinate (IRC) may be obtained through the reaction-path-following procedure incorporated in GAUSSIAN 90.

The ab initio free energy profile described above has been used to compute the potential of mean force (pmf) for the Menshutkin reaction in aqueous solution through Monte Carlo simulations with fitted empirical potential functions.¹⁴ Although the computed energetic results are in good agreement with the available experimental data, there is concern with the predicted transition-state structure in water because of the dramatic solvent effect.^{14,15} In the previous empirical approach, it was not possible to determine a priori the solvent effect on the change of the reaction profile in solution. The solvation free energy has to be evaluated separately and added to the free energy profile in the gas phase. Consequently, the maximum point on the free energy profile in solution will always be along the gas-phase MEP. Hence, the "TS" structure obtained this way is not necessarily the true saddle point on the *free energy surface* in solution. A proper treatment of the solvent effects on the TS structure should couple the solute-solvent interaction and the chemical process simultaneously and consider a two-dimensional free energy surface by treating both bond formation and breaking processes.

Fortunately, the combined QM/MM-AM1/TIP3P Monte Carlo simulation method provides a viable solution, and it is adopted in this study. To ensure that the AM1 method is appropriate to describe the Menshutkin reaction of H₃N + CH₃Cl, structural and energetic results are compared with the ab initio 6-31 + G(d) findings (Table II and Figure 2).¹⁴ Geometric variables for the reactant and product molecules predicted by the AM1 model are in excellent agreement with predictions by ab initio calculations at the 6-31 + G(d) level. The largest deviations are only 0.04 Å for the bond lengths and 1.3° for the bond angles. On the other hand, the AM1 model yields a much tighter TS structure than the ab initio approach. At the transition state, the C-N and C-Cl distances are 1.899 and 2.474 Å at the 6-31 + G(d) level, which are 0.24 and 0.23 Å longer than the AM1 values. In addition, the Walden inversion at the methyl group is about 3.8° more advanced in the AM1 structure. However, the ab initio geometric parameters appear to be somewhat overestimated for the Menshutkin reaction in view of the results for the S_N2 reaction of Cl⁻ + CH₃Cl, where the two C-Cl distances are 2.383 Å at the TS.⁵ In any event, since the primary interest of the present study is the solvent effect on the change in TS structure, it seems to be reasonable to use the AM1 geometry in fluid simulations. An alternative approach would be to use the ab initio potential surface for the Menshutkin reaction in the gas

**Figure 2.** Optimized AM1 and 6-31 + G(d) (in parentheses) geometries: bond lengths in angstroms and angles in degrees.**Figure 3.** Contour of the heat of formation for the Menshutkin reaction, H₃N + CH₃Cl → CH₃NH₃⁺ + Cl⁻, in the gas phase determined by AM1 calculations. The contour level is 2 kcal/mol. Values higher than 60 or less than -25 kcal/mol are not shown. Monte Carlo simulations are carried out within the rectangular region.

phase, supplementing solvation free energies evaluated with the AM1/TIP3P model.

The AM1 energy contour for the reaction H₃N + CH₃Cl → CH₃NH₃⁺ + Cl⁻ in the gas phase is shown in Figure 3. The feature of a shallow minimum for the product ion pair predicted by ab initio calculations is also revealed by the AM1 results.^{14,15} Note that although standard enthalpies are computed in the AM1 geometry optimization, the numerical results are actually in good agreement with free energy changes predicted at the MP4SDTQ/6-31 + G(d) level with 6-31 + G(d) vibrational frequencies (Table II). It appears that the AM1 results without entropic corrections provide a reasonable approximation to the ab initio free energy profile and thus will be used in the present study (see below).

(b) Bimolecular Interactions. The most crucial element in the simulation of chemical reactions in solute is the reliability of the method for computing intermolecular interaction energies at

(28) Computed from standard free energies of formation: -3.91 (NH₃), -14.38 (CH₃Cl), -57.40 (Cl⁻), and 149.2 (CH₃NH₃⁺). JANAF Thermochemical Tables, 3rd ed.; U.S. Government Printing Office: Washington D.C., 1971. J. Phys. Chem. Ref. Data Suppl. 1982; Vol. 11, 1985; Vol. 14. The value for CH₃NH₃⁺ was calculated from the process CH₃NH₂ + H⁺ → CH₃NH₃⁺; Aue, D. H.; Webb, D. H.; Bowers, M. T. J. Am. Chem. Soc. 1976, 98, 311. Lias, S. G.; Liebman, J. F.; Levin, R. D. J. Phys. Chem. Ref. Data 1984, 13, 695.

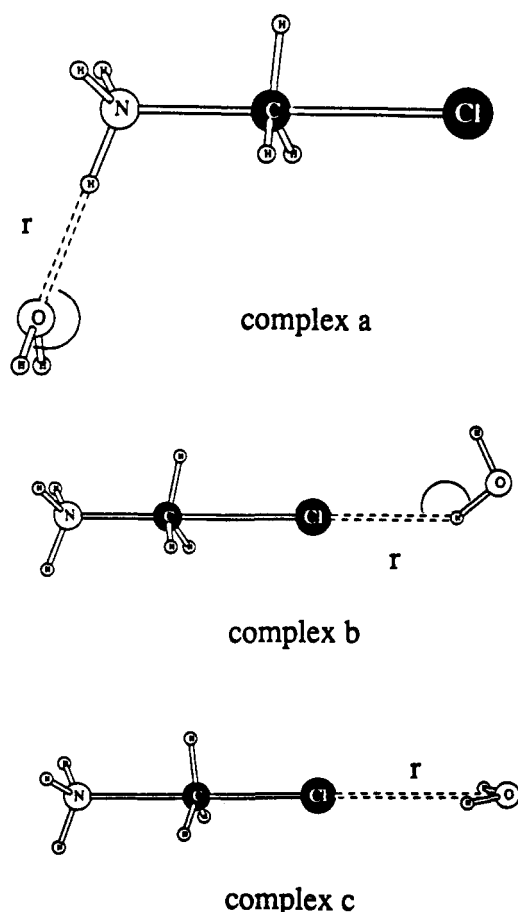


Figure 4. Structural arrangements of monohydrated clusters of $[H_3-CH_3-Cl]$.

different stages of the reaction; of course, it is, too, important for the solvent effects and associated boundary conditions to be correctly incorporated into the quantum Hamiltonian.¹² Consequently, geometries and interaction energies for solute–water complexes at different values of R_{CN} and R_{CCl} are computed at the ab initio 6-31 + G(d) level and are compared with predictions from the QM/MM model, through which the Lennard-Jones parameters (eq 2) are determined. Values of R_{CN} and R_{CCl} are chosen along the 6-31 + G(d) MEP corresponding to RCs of $-1.5, -1.0, -0.5, -0.25, -0.1, 0.0, 0.1, 0.25, 0.5$, and 0.75 . The ab initio results for these bimolecular complexes with water have been used to derive the empirical potential function employed in our previous study of the Menshutkin reaction in water.¹⁴ At each of the selected points, two or three configurations of the solute–water complex are considered. Figure 4 depicts the structural arrangement of these bimolecular complexes. Structure a specifies the hydrogen-bonding interaction between the ammonium hydrogen and the oxygen of water, while complexes b and c denote the open and bifurcated forms between water and Cl. In all geometry optimizations (ab initio, QM/MM, and empirical), monomer geometries are fixed at the 6-31 + G(d) and experimental values for the reactants and water, respectively, while hydrogen-bonding parameters that are optimized are indicated in Figure 4. At the 6-31 + G(d) level, complex a has the strongest binding energy along the whole RC, whereas complex c forms the weakest complex of the three structures considered.

The ab initio interaction energies are first compared in Figure 5 (top) with those predicted by the empirical potential function used in ref 14. As expected, hydrogen-bonding interactions exhibit a gradual increase along the reaction coordinate. Excellent agreement is obtained with a root-mean-square (RMS) deviation of 0.4 kcal/mol between the two methods; however, the parametrization procedure was laborious and required a cubic spline

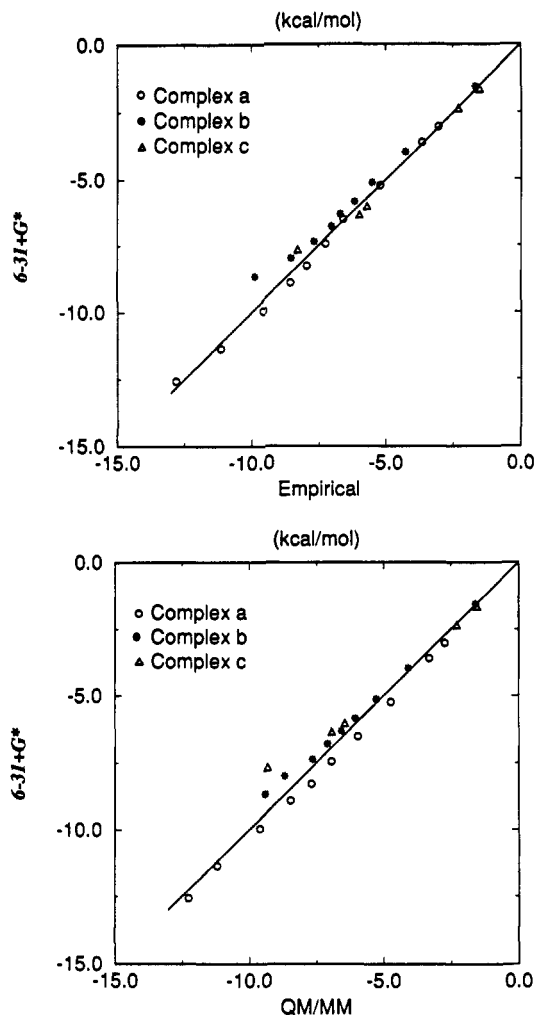


Figure 5. Comparison of the solute–solvent interaction energies predicted by the potential functions (top) and by the AM1/TIP3P model (bottom) vs the 6-31 + G(d) values. A line of slope = 1.0, indicating perfect agreement, is shown. All energies are in kilocalories per mole.

technique to specify the changes of the potential function parameters along the RC.¹⁴ It is perhaps not even practical to derive such empirical potentials for the reaction surface considered here because the empirical parameter fitting would require consideration of bimolecular interactions spreading over the entire potential surface.⁸ In contrast, the solute–solvent interaction is naturally determined in the combined QM/MM treatment.^{12,16} Figure 5 (bottom) correlates the QM/MM prediction and the ab initio 6-31 + G(d) results. In these calculations, the solute, $[H_3N-CH_3-Cl]$, is treated quantum-mechanically, while water is represented by the TIP3P model. The accord is good for an energy range of -1 to -12 kcal/mol; the overall RMS deviation is 0.5 kcal/mol. Large deviations between the QM/MM and 6-31 + G(d) results are mainly from complex c, without which the RMS deviation would be 0.4 kcal/mol. The agreement demonstrated here provides strong support for the use of the QM/MM method to study the Menshutkin reaction in aqueous solution.

Free Energy Surface in Aqueous Solution

The principal goal of the present study is to determine the solvent effect on the potential surface of the Menshutkin reaction in water. This can be achieved by using statistical perturbation theory in Monte Carlo or molecular dynamics simulations. It is, of course, straightforward to compute the potential of mean force for the reaction along a predefined one-dimensional reaction path;^{5,14} however, the construction of the potential surface requires

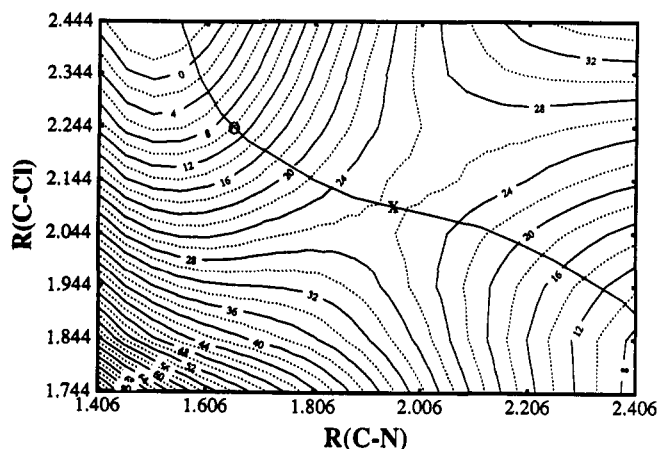


Figure 6. Computed free energy surface for the Type II S_N2 reaction $[H_3N-CH_3-Cl]$ in aqueous solution as a function of C-N and C-Cl separations. The transition state is marked by an X, while the minimum energy path defined by eq 5 is indicated by the curve across the diagram. Energies are given in kilocalories per mole, and distances are in angstroms.

knowledge of relative free energies of all grid points (Figure 1) on the two-dimensional map.²⁵ This is a substantial undertaking in computational effort, especially with the use of the combined QM/MM potential. Consequently, emphasis is centered on the region indicated in Figure 3, where bond forming and breaking in the Menshutkin reaction take place. The results are shown in Figure 6, in which the saddle point at $R_{CN} = 1.96$ Å and $R_{CCl} = 2.09$ Å is marked by an X, while that in the gas phase is indicated by an O.

Several technical points should be addressed before the results are discussed further. First, in the present QM/MM approach, it is possible to decompose the computed total free energy change between two adjacent grid points into the intrinsic (gas-phase) contribution and the free energy of hydration.²⁹ This is accomplished by writing the quantum mechanical energy of given C-N and C-Cl distances $E_{QM}(R_{CN}, R_{CCl})$ (eq 3) in terms of the gas-phase energy and an energy penalty required to polarize the electron distribution in solution:^{16,29}

$$E_{QM}(R_{CN}, R_{CCl}) = E^o_{gas}(R_{CN}, R_{CCl}) + \Delta E_{dist}(R_{CN}, R_{CCl}) \quad (6)$$

Here, $E^o_{gas}(R_{CN}, R_{CCl}) = \langle \Phi^o | H^o_{QM}(R_{CN}, R_{CCl}) | \Phi^o \rangle$, and $E_{QM}(R_{CN}, R_{CCl}) = \langle \Phi | H^o_{QM}(R_{CN}, R_{CCl}) | \Phi \rangle$, which are the electronic energies of the reactants in the gas phase and in water. ΔE_{dist} is the electron distortion energy due to solute-solvent interactions,^{16,29} and Φ^o and Φ are the wave functions of the solute in the gas phase and in water, respectively. Thus, the solvation free energy for the Menshutkin reaction can be determined by subtracting the gas-phase potential (Figure 3) from the aqueous free energy surface (Figure 6) obtained via the QM/MM simulations. It should be emphasized that the combined QM/MM approach has the advantage of taking into account of the solvent polarization effects that are partially reflected by the ΔE_{dist} term.¹⁶ Generally, this is of great concern if pairwise, empirical potential functions are used.

Second, the enthalpy change computed with the AM1 method is used here to approximate the free energy surface for the reaction of $H_3N + CH_3Cl$ in the gas phase. Table II shows that the approximation is quite reasonable since the estimated enthalpy of activation (50 kcal/mol) is in reasonable accord with the free energy predicted at the MP4SDTQ/6-31 + G(d) level (47 kcal/mol). However, the AM1 method overestimates the energy of reaction for the Menshutkin reaction by 18 (27) kcal/mol compared with the ab initio (experimental) data.²⁸ The discrepancy is largely due to the poor performance of the AM1

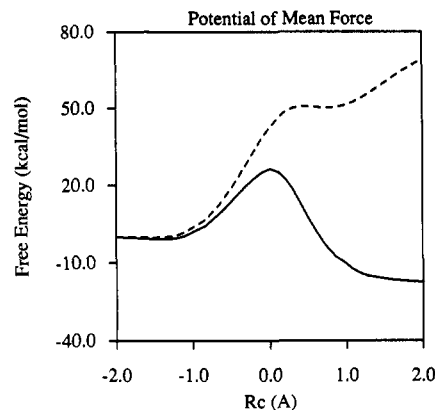


Figure 7. Potential of mean force for the Menshutkin reaction in water (solid curve) and in the gas phase (dashed curve). The reaction coordinate is the minimum energy path shown in Figure 6.

theory for the chloride ion, whose heat of formation is predicted to be 18.2 kcal/mol higher than the experimental number.¹⁷ This difference is expected to be fully transferred into the results from the QM/MM Monte Carlo simulation; however, it is not expected to affect the energetics in the region before/near the transition state.

Finally, a major concern in the present study is the choice of the independent variables for the reaction surface. A linear approach of the nucleophile to CH_3Cl is assumed, which appears to be reasonable; however, a full description of the reaction surface should also include the angular averaging of the nucleophilic attack. Extension beyond the present two-dimensional surface that treats the C-Cl and C-N variations independently is unfortunately beyond our current computational capability. Note that classical trajectory studies of the Type I S_N2 reactions with a box of solvent molecules have been carried out by Gertner et al.^{7b} and by Hwang et al.,^{6d} while Tucker et al.⁸ used a multidimensional transition-state theory, but included only a few solvent molecules. It is of interest to perform similar calculations using the present QM/MM approach.

The most striking finding in Figure 6 is the shift of the TS structure that accompanies a dramatic solvent stabilization of the products. This finding is in good agreement with the prediction based on the Hammond postulate.¹³ The structural change features a lengthening of the C-N distance of 0.30 Å from its gas-phase value of 1.66 Å and a decrease in the C-Cl bond length by 0.15 Å (2.09 Å in water). Therefore, the TS of the Menshutkin reaction occurs much earlier in aqueous solution than in the gas phase. For comparison, structural changes predicted in our previous investigation using empirical potentials are +0.15 and -0.10 Å for R_{CN} and R_{CCl} , respectively.¹⁴ However, that work differs from the present investigation in two ways: (1) there is no relaxation of the electronic structure allowed during the simulation and (2) the gas-phase MEP is held fixed without consideration of the symmetric stretch along the reaction path.^{5c} The structural change is entirely due to solvation without consideration of electronic structure relaxation.¹⁴ The present QM/MM method, on the other hand, allows electronic relaxation of the reactants on a two-dimensional free energy surface in aqueous solution through the quantum Hamiltonian.¹⁶ Consequently, a much more dramatic solvent effect is observed. Note that a similar Menshutkin reaction involving H_3N and CH_3Br has been studied by Solà et al., using a continuum self-consistent reaction field method in ab initio molecular orbital calculations.¹⁵ They found similar qualitative features for the TS structure when a dielectric constant of 78 was used to represent the aqueous solution.

Figure 7 illustrates the pmf along the reaction path shown in Figure 6 for the Menshutkin reaction, which has been extended by additional calculations along the path leading to the reactants

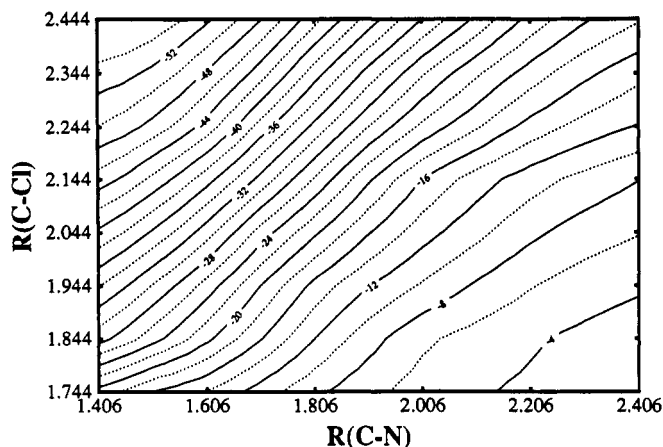


Figure 8. Free energy of hydration for the Menshutkin reaction in water. Energies are given in kilocalories per mole relative to the reactants at an $RC = -2 \text{ \AA}$.

and products. The RC of Figure 7 is defined by eq 5, but the TS structure in aqueous solution (Figure 6) is used to specify the reference state for RC_0 . In Figure 7, the pmf is zeroed at $RC = -2.0 \text{ \AA}$, which is virtually flat for $|RC| \geq 1.0 \text{ \AA}$, suggesting that the SCF-type calculation can provide reasonable estimates for the energetics for the entire Menshutkin reaction, including the entrance and exit channels. It should be mentioned that the potential surface shown in Figure 6 is also anchored relative to this point ($RC = -2.0 \text{ \AA}$). The calculated free energy of activation is $26.3 \pm 0.3 \text{ kcal/mol}$ in water. Experimental data do not appear to be available for this particular system, perhaps due to practical difficulties in using gaseous CH_3Cl to carry out these experiments; however, the result is in accord with the experimental activation energy (23.5 kcal/mol) for a similar reaction between $\text{H}_3\text{N} + \text{CH}_3\text{I}$ in water³⁰ and the previously computed value of 25.6 kcal/mol .¹⁴ The agreement further supports the utilization of the combined QM/MM-AM1/TIP3P potential in the present study. For comparison, an activation energy of 8.3 kcal/mol was predicted by Solà et al. for $\text{H}_3\text{N} + \text{CH}_3\text{Br}$, which appears to be too small,¹⁵ indicating that specific consideration of solute-solvent interactions is important for the present type II S_N2 reaction.

Figure 7 also gives the free energy of reaction, ΔG_{rxn} , in water ($-18 \pm \text{kcal/mol}$), which represents a solvent stabilization of about 155 kcal/mol relative to the gaseous process. The latter value is in exact agreement with the prediction of ref 14. The experimental estimate of ΔG_{rxn} from a thermodynamic cycle, using free energies of hydration and standard free energies of formation, is about $-34 \pm 10 \text{ kcal/mol}$.¹⁴ As mentioned above, the AM1 model overestimates the heat of formation of Cl^- by 18 kcal/mol .¹⁷ If the experimental value were used, the computed reaction free energy would be -36 kcal/mol . The calculations by Solà et al. yield values of -27 to -44 kcal/mol with different basis sets.¹⁵

A detailed consideration of the free energy surface sheds light on the nature of the Menshutkin reaction in water. The attack of H_3N toward the substrate leads to a charge separation to yield methylammonium and chloride ions. The process is extremely unfavorable in the gas phase due to Coulombic interactions. Indeed, Menshutkin reactions have never been reported in the gas phase.³¹ However, in aqueous solution, the reactants become better and better solvated as the reaction proceeds, eventually leading to an exothermic process.^{1,4a} The contour of the free energy of hydration is depicted in Figure 8, which shows a continuous enhancement of the reaction toward products. Therefore, the balance between the increase in energy due to

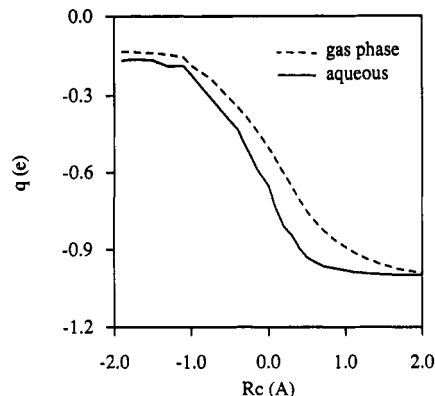


Figure 9. Comparison of the average charge transfer in aqueous solution (solid curve) and in the gas phase (dashed curve) along the reaction coordinate for $\text{H}_3\text{N} + \text{CH}_3\text{Cl}$. Partial charges for the leaving group (Cl) are given in electrons. Standard errors for the computed atomic charge in water are about 0.005 e .

charge separation during the reaction and the favorable solvation effects result in a shift in the position of the transition state and a reduction of the free energy of activation. Analogously Solà et al. used a Shaik-type state correlation diagram to rationalize the solvent effects on the change of the TS structure.^{15,32} It is also interesting to notice that the pmf in Figure 7 corresponds to a unimodal energy profile in aqueous solution, which is consistent with the traditional notion of S_N2 reactions and with the prediction from the empirical approach.^{1,14,15}

Differential Solvation on the Reactants and the Transition State

(a) Atomic Charges. Additional insight into the solvent effect can be obtained by analyzing the extent of charge transfer during the reaction in the gas phase and in aqueous solution. The computed Mulliken population charges for the leaving group (Cl) along the reaction path of Figure 7 for both the gas-phase and the aqueous processes are shown in Figure 9, since it gives a good indication of the charge development during the reaction. Charge-population analyses have been performed by Bash et al.^{6c} and by Hwang et al.^{6d} in their molecular dynamics calculation of the reaction, $\text{Cl}^- + \text{CH}_3\text{Cl} \rightarrow \text{CH}_3\text{Cl} + \text{Cl}^-$, using the combined AM1/TIP3P potential and an EVB approach.^{6c} Similar calculations have been performed for other systems.^{7,12b,14,33} In contrast to the findings by Bash et al. for the Type I process, where charge transfer in water lags behind the process in the gas phase,^{6c} the Type II reaction exhibits a solvent-promoted charge separation due to stabilization by interacting with the solvent molecules. This is, of course, consistent with the observed solvent effect on the activation energies for these reactions. For the Menshutkin reaction, a charge separation of more than 65% at the transition state in water is predicted from the QM/MM-AM1/TIP3P simulation, whereas it is only about 50% in the gas phase. It should be pointed out that although the Mulliken population analysis only gives a "rough" estimate of the charge distributions, the qualitative trends are still informative. Interestingly, the partial charge used in the empirical potential is about 0.7 e on the chlorine atom at the TS.¹⁴

(b) Energy Distributions. Details of the solute-solvent interaction are provided in Figure 10, which shows the distribution of pair interaction energies between the solute and water molecules. Three distributions, corresponding to the reactants ($RC = -2 \text{ \AA}$), TS ($RC = 0 \text{ \AA}$), and products ($RC = 2 \text{ \AA}$), are shown. As expected, the neutral reactant molecules interact weakly with the solvent without any specific structural features, while the

(30) (a) Okamoto, K.; Fukui, S.; Shingu, H. *Bull. Chem. Soc. Jpn.* **1967**, *40*, 1920. (b) Okamoto, K.; Fukui, S.; Nitta, I.; Shingu, H. *Bull. Chem. Soc. Jpn.* **1967**, *40*, 2354.

(31) Abraham, M. H. *Prog. Phys. Org. Chem.* **1974**, *11*, 1.

(32) Shaik, S. S. *Prog. Phys. Org. Chem.* **1985**, *15*, 197.

(33) (a) Cramer, C. J.; Truhlar, D. G. *Science* **1992**, *256*, 213. (b) Tapia, O.; Colonna, F.; Angyan, J. G. *J. Chim. Phys.* **1990**, *87*, 875.

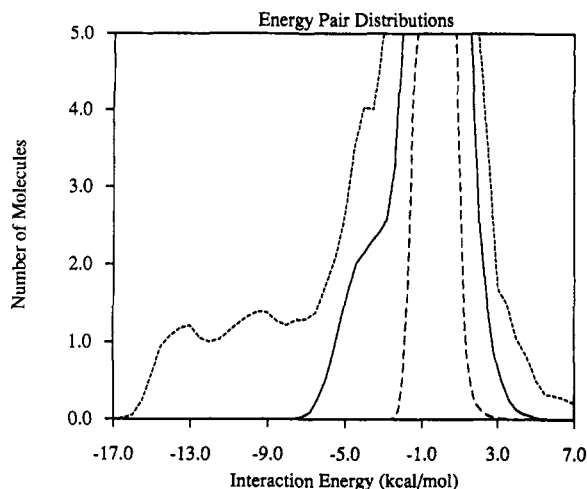


Figure 10. Computed solute-solvent energy pair distributions for the reactant (dashed curve), transition state (solid curve), and product (dotted curve). The ordinate gives the number of water molecules bound by the solute, with the energy shown on the abscissa. Units for the ordinate are molecules per kilocalories/mole.

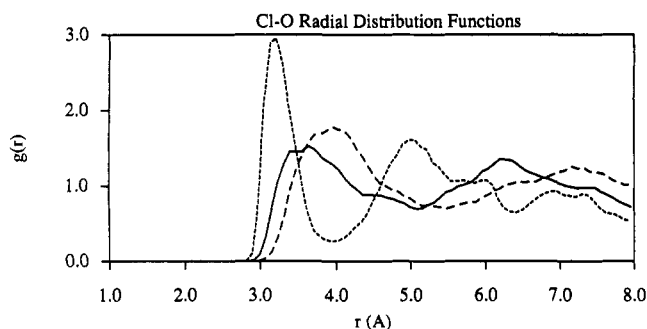


Figure 11. Computed Cl-O radial distribution functions. Dashed curves are for the reactant, solid curves are for the transition state, and dotted curves are for the product. This convention is used throughout.

striking pike centered at $E_{\text{int}} = 0$ kcal/mol is due to interactions with distant water molecules. Although ammonia is a good hydrogen bond acceptor, the close proximity of the substrate prevents water from forming a hydrogen bond to the lone pair of electrons on the nitrogen atom. On the other hand, it is well known, both from gas-phase microwave experiments and theoretical investigations, that ammonia is a poor hydrogen bond donor.³⁴ The pair energy distribution is thus consistent with bimolecular interactions shown in Figure 6. At $RC = -2$ Å ($R_{\text{CN}} = 3.5$ Å), the best reactant-water interaction energy is -2.6 kcal/mol. For the transition state, a hydrogen-bonding band begins to develop (solid curve in Figure 10). The best interaction energy from Figure 10 for the TS is -7.6 kcal/mol. Finally, two low-energy bands are clearly seen for the product ion pair (dotted curve). The lowest energy band can be assigned to water molecule solvating the ammonium ion, while the second peak is for the chloride ion-water complex. In fact, the low-energy bands can nearly be superimposed with pair energy distributions for $\text{CH}_3\text{-NH}_3^+$ and Cl^- obtained from separate simulations.

Integration of the dotted curve to -12.0 kcal/mol yields about 3.7 water molecules, whereas integration of the second band from -12.0 to -8.0 kcal/mol reveals another 5 water molecules. The total number of the water molecules resulting from the first and second peaks is 8.7, which consists of approximately three $\text{CH}_3\text{-NH}_3^+$ -water pairs and six Cl^- -water pairs. An important observation is that the number of strong hydrogen-bonding

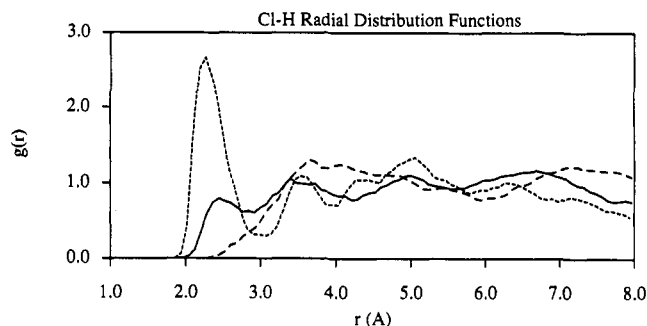


Figure 12. Computed Cl-H rdfs.

interactions increases from 0 for the reactants at $RC = -2$ Å to about 9 for the product ion pair. It is noteworthy to recall findings for the Type I reaction of $\text{Cl}^- + \text{CH}_3\text{Cl}$ in water, where the number of hydrogen bonds is roughly constant along the whole reaction path.^{5a} The differential solvation for the reactants and the transition state in that study is due to variations in the strength of the hydrogen bonds.^{5a} In contrast, increases both in the total number of hydrogen bonds and the strength of interaction energies are critical to the stabilization of the TS and products for this Type II $\text{S}_{\text{N}}2$ reaction in aqueous solution.

(c) Radial Distribution Functions. The solute-solvent structure can be further characterized by the radial distribution functions (rdfs) shown in Figures 11–15. In these figures, the first atom for an xy distribution, $g_{xy}(r)$, refers to a solute atom, and the second atom is either the hydrogen or the oxygen of water. The rdf $g_{xy}(r)$ gives the probability of finding an atom y at a distance r from atom x . Here, the dashed, solid, and dotted curves correspond respectively to the reactants ($RC = -2$ Å), TS ($RC = 0$ Å), and the products ($RC = 2$ Å) in aqueous solution.

The Cl-O and Cl-H distributions in Figures 11 and 12 reveal the progress of hydrogen-bonding interactions between chlorine and water during the reaction. The positions of the first peaks in the Cl-O rdfs (Figure 11), are 4.0, 3.6, and 3.2 Å for the reactant, TS, and product, respectively, indicating strengthened interactions with the solvent in the series. The trend is unambiguously demonstrated by the Cl-H rdfs in Figure 12 by the appearance of the hydrogen bond peak at 2.4 Å for the transition state and the striking first peak at 2.3 Å for the product chloride ion. The reactant methyl chloride shows no hydrogen-bonding interactions between Cl and water, consistent with previous findings by Chandrasekhar et al. using empirical potential functions.^{5a} Note that for the product ion-pair structure, there is also a well-defined second solvation shell centered at 3.5 Å in the Cl-H rdf, while the third peak near 5 Å can be assigned to water molecules forming hydrogen bonds with the ammonium ion. Integration of the first peaks for the product and TS to their minima at 3 Å reveals 6.6 and 3.1 nearest neighbors forming hydrogen bonds with the chlorine atom. This is in accord with the prediction based on the integration of the pair energy distributions, where the number of hydrogen bonds to the chlorine atom is estimated to be about 6 for the product.

Similar trends exist for hydrogen-bonding interactions between the nucleophile H_3N and water. In the ammonia $\text{H}_\text{N}\text{-O}$ rdfs (Figure 13), there is no strong interaction between the ammonia hydrogen and the oxygen of water (dashed line), while a shoulder in the distribution at the hydrogen-bonding range occurs for the transition state (solid curve). Integration of the sharp first peak centered at 1.8 Å for the product gives 1.0 hydrogen bonds. Thus, there are a total of 3 water molecules hydrogen-bonded to the ammonium ion. The progression of hydrogen bonding with the ammonia group is also indicated by the N-O rdfs given in Figure 14. Note that the location of the sharp first peak for the product ion pair (2.8 Å) is about 1 Å (N-H bond length) longer than the first peak in the $\text{H}_\text{N}\text{-O}$ rdf.

(34) (a) Nelson, D. D., Jr.; Fraser, G. T.; Klemperer, W. *Science* **1987**, *238*, 1670. (b) Del Bene, J. E. *J. Phys. Chem.* **1988**, *92*, 2874. (c) Frisch, M. J.; Del Bene, J. E.; Binkley, J. S.; Schaefer, H. F., III *J. Chem. Phys.* **1986**, *84*, 2279.

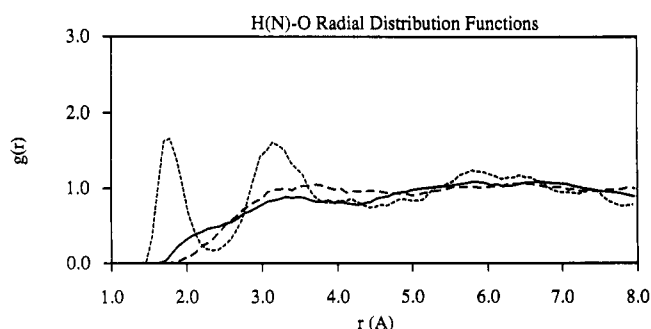


Figure 13. Computed ammonium hydrogen–water oxygen rdfs.

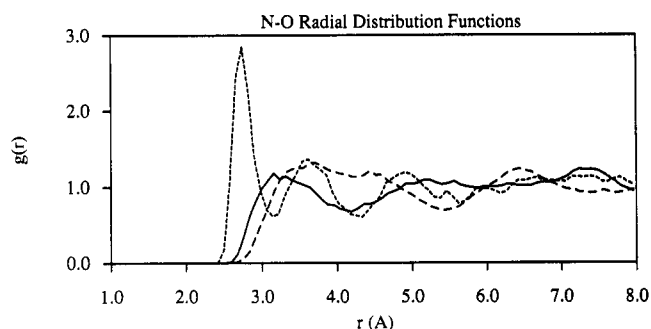


Figure 14. Computed N–O rdfs.

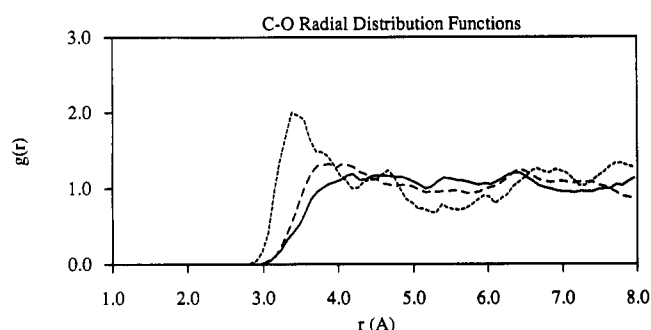


Figure 15. Computed C–O rdfs.

The C–O (Figure 15) rdfs may give some indication of the change in solvation at the methyl group that is being attacked by the nucleophile. However, no special features exist in these plots, especially for the reactant and transition state. Note that a strong first peak is shown in the C–O rdf for the product. This is perhaps due to electrostatic interaction between the ammonium ion and water, which have been observed for hydrophobic cations in water.³⁵ Comparing g_{NO} (Figure 14) with g_{CO} (Figure 15), two differences are apparent: (1) the distances in the carbon–water oxygen rdfs are much longer than those in the nitrogen–water oxygen rdfs and (2) the change in the rdf on going from the reactant to the product is less dramatic for g_{CO} than for g_{NO} . Both observations suggest that the interaction between the methyl group and water is weak throughout the reaction.

Conclusions

A comprehensive study of the Type II S_N2 reaction between H_3N and CH_3Cl in aqueous solution has been carried out through

(35) Jorgensen, W. L.; Gao, J. J. *Phys. Chem.* **1986**, *90*, 2174.

statistical mechanical Monte Carlo simulations using the combined quantum mechanical and molecular mechanical AM1/TIP3P potential. The endothermic Menshutkin reaction in the gas phase is strongly enhanced by the influence of aqueous solvation. This stems from the fact that a charge separation is developed in the course of the reaction, giving rise to favorable solvent stabilizations. The reaction becomes exothermic in water. The computed free energy of activation and free energy of reaction are in good agreement with experiment.

A major thrust of the present study is to characterize the solvent effect on the potential surface and the transition-state structure for the Menshutkin reaction. Thus, a two-dimensional free energy surface has been determined. The present study has the advantage of taking into account the effect of solute electronic structural relaxations, while the symmetric stretch along the reaction path is being considered through the grid search. In accord with previous theoretical studies and the empirical expectation according to the Hammond postulate, an early transition state is predicted in aqueous solution for the type II S_N2 reaction, with a dramatic increase in the C–N distance by 0.30 Å and a decrease in the C–Cl separation by 0.15 Å at the transition state. When the gas-phase minimum energy path was used to approximate the reaction path in water, the change for C–N and C–Cl was predicted to be +0.15 and –0.10 Å, respectively.¹⁴ Clearly, solvent effects should be included in electronic structure calculations for asymmetric reactions in condensed phases. The combined QM/MM simulation method as demonstrated here and in other works provides a viable approach.

The present calculations also illustrate the power of the combined QM/MM Monte Carlo simulation method in providing both qualitative and quantitative insights into the solvent effects on chemical reactions. In the past decade, computer simulations have greatly enhanced our understanding of chemical processes and intermolecular interactions in solution. These techniques have been extended to enzymatic reactions. In the past, these calculations were performed primarily with the use of effective pairwise potential functions. Although the classical approximation is quite reasonable and can provide valuable information on solute–solvent interactions, the coupling between the solvent charge distribution and the solute electronic polarization, which is of central importance for reactions involving heterolytic bond cleavage,^{6d,12} is not specifically considered. Further, it is generally not practical to fit parameters for a potential surface such as the one studied here. Using the combined QM/MM approach, we anticipate that a variety of chemical processes, both in solution and in enzymes, will be investigated with ease.

Acknowledgment. Gratitude is expressed to the National Science Foundation Supercomputing Center and the Pittsburgh Superconducting Center for computational support. X.X. thanks Professor T. George for encouragement. We thank Professor W. L. Jorgensen and Dr. J. J. P. Stewart for making their programs available, each of which forms an integral part of the procedure described here. Both referees provided valuable comments.

Supplementary Material Available: Computed free energy changes from the QM/MM simulations and geometrical and energetic results for the solute–water complexes determined with the 6-31 + G(d) basis set, the empirical potential function, and the combined AM1/TIP3P method (7 pages). Ordering information is given on any current masthead page.